Soft Snake Robots: Mechanical Design and Geometric Gait Implementation

Callie Branyan[1,*], Chloë Fleming[1,*], Jacquelin Remaley[1], Ammar Kothari[1],
Kagan Tumer[1], Ross L. Hatton[1], and Yiğit Mengüç[1,†]

[1]Robotics Program, School of Mechanical, Industrial, and Manufacturing Engineering, Oregon State University
[*]Equally contributing co-authors
[†]yigit.menguc@oregonstate.edu

***Abstract*— Soft robots are compliant and durable, and thus potentially better-suited for swimming or crawling over rough terrain than conventional rigid robots. Biomimetic locomotion strategies are often implemented on soft robots, but are difficult to tune because of the complexity of mapping nonlinear mechanical systems to specific gait patterns. We propose an approach to soft robot control in which the robot is designed to physically realize a shape space (mechanically predefined body poses) to follow a theoretically optimal gait. Specifically in this paper we present an entirely soft snake robot designed to implement the prerequisite shape space for slithering gaits. When coupled with a geometric mechanics model relating serpentine shape sequences to displacement, appropriate gait patterns can be selected analytically based on the system's Lie bracket. We developed a modular, two-link soft robot and used the geometric mechanics model to identify several cyclic gait patterns for producing forward displacement. The gait patterns were tested on the soft robot and observed with a motion capture system to measure displacement and monitor shape sequences. Relative performance of the gait patterns is consistent with the geometric "soap-bubble method" as a heuristic for gait optimization, which demonstrates the applicability of this approach to soft robot control and coordination.**

I. Introduction & Related Work

Recent developments in soft robotics have expanded the possibilities of building biomimetic systems that are flexible, dynamic, and more robust in complex environments than their rigid counterparts. Soft robots are often composed of elastomeric actuators that are capable of continuum bending. This property makes them suitable for tasks in unstructured environments in which they can leverage the locomotion strategies of fish, snakes, and other animals that are relatively unconstrained by rigid skeletons. These examples from nature are high degree of freedom (DOF) systems that are difficult to approximate with rigid parts. For instance, snake robots have traditionally been built from a series of high DOF rigid actuators to produce sufficient bending capabilities. Although these efforts have been successful in demonstrating effective locomotion methods inspired by the gaits of real snakes, their movement requires a complex control system and is ultimately constrained by their inelastic bodies. The contributions we present in this work are two-fold: the mechanical design of a soft robot for undulatory locomotion, and demonstrating the utility of geometric mechanics to identify appropriate gaits for a soft continuum robot.

Snakes use a variety of strategies to achieve forward locomotion depending upon the composition of their habitats.

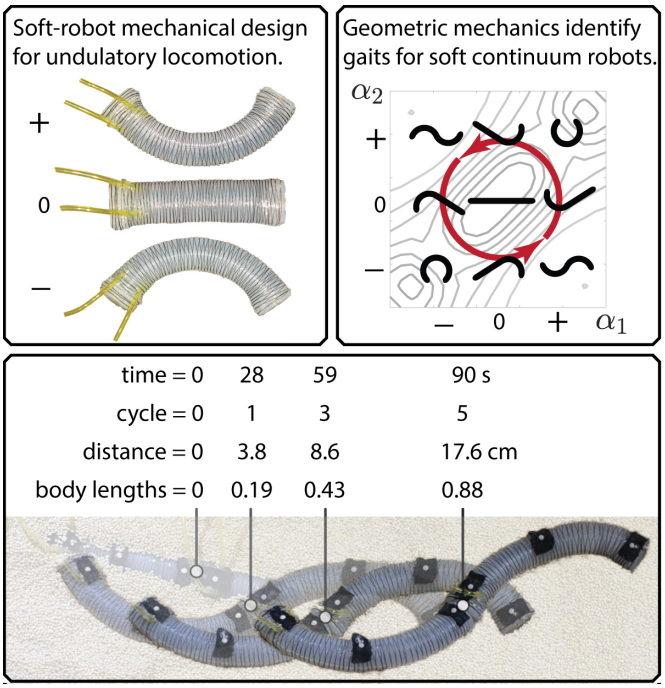

Fig. 1: The contributions of this work are two-fold: the mechanical design of soft-robotic actuators for undulatory locomotion, and the use of geometric mechanics to identify good candidate gaits for a soft continuum robot.

The most recognizable gait is *lateral undulation*, also known as serpentine locomotion or slithering [1]. This method requires a propagation of lateral bending along the snake's backbone, utilizing a resultant force vector to propel the snake forward upon surface contact. This gait does not itself result in forward movement without sufficient friction generated against the ground surface to produce lateral resistance, which is usually provided by anisotropic scales on the snake's underside. The need for scales is obviated when the ground medium has fluidic properties that produce a relatively high and anisotropic drag coefficient, such as water or sand [1].

Soft robots are difficult to control due to their intrinsic nonlinear behavior, and developing control strategies for soft robots is still a nascent area of research. Two primary approaches to this challenge have emerged in recent works: developing comprehensive system dynamics models to in-

corporate into a control algorithm, and empirically designing soft mechanical systems to execute specific gait patterns. The first approach includes strategies such as recursive estimation of dynamics [2], low frequency Finite Element Analysis in real time [3], and training neural networks to yield an inverse kinetics function [4]. Most of these efforts focus on discovering forward or inverse mappings between actuator input and shape, and do not address the more complex issue of identifying and controlling shape sequences to produce an effective gait. Alternatively, evolutionary/learning algorithms can be used either to provide efficient gait "actions" directly [5], or to search through the parameters of a predetermined gait profile [6].

Empirically pre-programming the locomotion strategy in mechanical design has proven to be successful for many soft robots, including early works demonstrating quadruped gaits in [7] and [8]. More recently, a few groups have implemented effective biomimetic peristalsis gaits inspired by earthworms [9] and caterpillars [10] by centering the control strategy around a mechanical design that produces a gait pattern with simple actuation sequences. Our work builds upon this approach by designing a soft system that can assume a set of poses in the serpentine *shape space* to implement tunable gait patterns available to snake-like robots.

Snake robots have long been of interest to the robotics community for their applications in field robotics and confined spaces, and thus locomotion strategies for serpenoid robots are well-studied. Many biological snake gaits can be described as sinusoidal waves of bending propagating along the backbone in the ground and vertical planes, which creates lateral undulation and shifting contact points with the ground [11], [12]. A primary goal of geometric mechanics locomotion research is to quantify displacement as a function of such changes in body shape for simple snake-like systems [13]. Continuum bending can be approximated by a *hyper-redundant* system of rigid parts [14], which is the prevailing approach to implementing a snake-like robot. The most successful snake robots to date have been based on a design consisting of many modules actuated by servos and connected in series, with a rotational offset between adjacent modules to produce sinusoidal shapes in the ground and vertical planes [15]–[17]. Generating control algorithms based on the inverse kinematics of a hyper-redundant rigid robot is not a trivial task [14], [18], with challenges such as composing wave functions from key poses and mapping these functions to actuators in the snake's body [19]. One recent work implemented a lateral undulation gait in a soft robot, although they mounted these actuators on wheels to generate anisotropic friction between the soft body and hard surface for forward motion [20].

This paper proposes driving the design and control of an entirely soft snake robot based on a shape space derived from a geometric mechanics model for generating serpentine gaits. We define a two-dimensional shape space that encompasses a subset of serpentine shapes and derive a soft robot design from this definition that can assume a set of poses on this space. We developed silicone, pneumatic actuators that

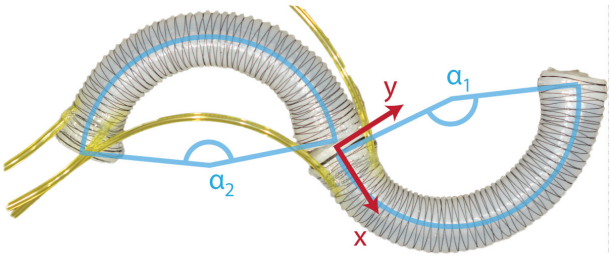

Fig. 2: Geometry of shape variables in two-actuator soft snake system. The origin of the body frame coordinate system is placed at the center point along the spine between the two actuators, with the x-dimension of position parallel to the spine and y-dimension perpendicular. The turning angle θ is defined relative to the x-axis.

are inexpensive, easy to manufacture, and capable of high-curvature continuum bending to realize pose sequences that compose a slithering gait using only a pair of antagonistic actuators. In addition, the actuators have a modular design and can be connected in series with embedded magnets, which offers the opportunity to produce more elegant backbone shapes for lateral undulation to be explored in the future.

Section II of this paper discusses the theory behind the geometric mechanics model used to inform the gait selection for the soft robot. Section III describes the actuator design choices and manufacturing process. The methodology for controlling and testing gaits is described in Section IV, and these results are compared with the outcomes predicted by the geometric mechanics model in Section V. Analysis of the project and plans to build upon these efforts are discussed in Section VI.

II. Snake Gait Selection

A primary goal of this work is to demonstrate the effectiveness of using a well-defined geometric gait model to develop a control sequence for a soft robot, and to show that this strategy can be separated from the nonlinear dynamics through which the system achieves the sequence of shapes. Our selection of shape sequences that are likely to form an effective gait is guided by the soap-bubble [21] model of gait performance which geometrically balances the displacement achieved over a gait cycle against the cost (measured in time or effort) required to execute that cycle.

The pose set for backbones of biological snakes can be represented by sinusoidal traveling wave functions [11], [19]. The *serpenoid-curve gait* for this system can be specified by the amplitude of sine and cosine curvature modes [21]. Our soft snake robot is a two-link, piecewise-continuous-curvature system which can approximate a subset of the biological snake's backbone shape space and thus can implement locomotion with select serpenoid-curve gaits. The soft robot's shape space can be parameterized by the arc angle of each link, α_1 and α_2. See Fig. 2 for an illustration of these shape parameters on the robot's body and Fig. 3(a) for example backbone shapes produced by varying α_1 and α_2. Displacement and orientation of the robot are measured as the displacement of the *body frame*, a coordinate system

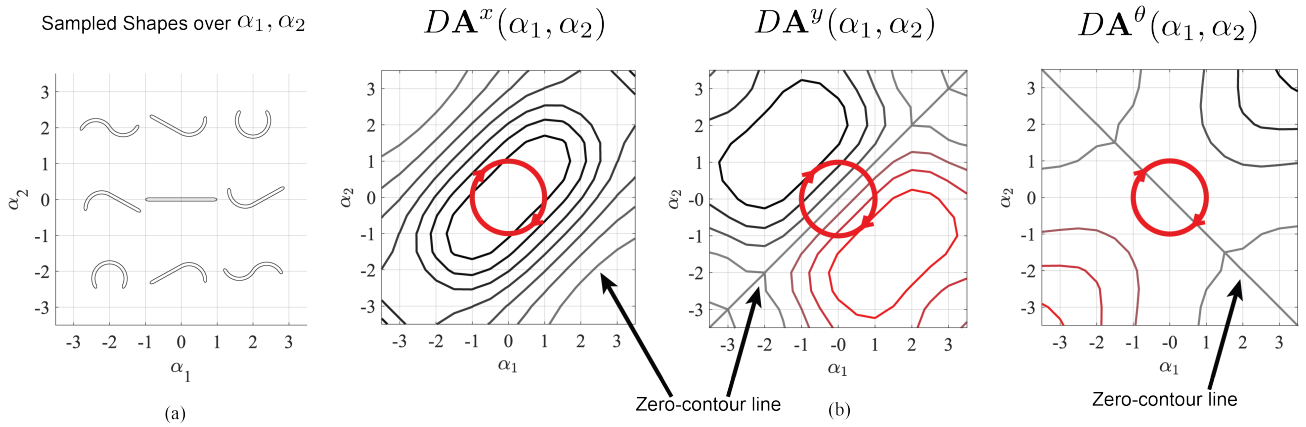

Fig. 3: (a) Sampled backbone shapes for the soft serpenoid system visualized as a function of α_1 and α_2. (b) Constraint curvature ($D\mathbf{A}(\alpha_1, \alpha_2)$) for the soft serpenoid system in a granular substrate with a lateral-to-longitudinal drag ratio of 1.8 to 1, visualized as contour plots with respect to x, y, and θ. An example gait stroke that varies α_1 and α_2 sinusoidally and 90 degrees out of phase to produce a "circular" stroke is plotted. Note that the gait cycle encloses part of a sign-definite region $D\mathbf{A}^x(\alpha_1, \alpha_2)$, indicating that there will be net displacement per cycle along the longitudinal axis of the body. The gait cycles encloses equal positive and negative regions on the contours $D\mathbf{A}^y(\alpha_1, \alpha_2)$ and $D\mathbf{A}^\theta(\alpha_1, \alpha_2)$ and thus will not produce any lateral or rotational displacement.

positioned at the center of the spine at $t = 0$ as shown in Fig. 2, from its initial position.

The configuration of the soft snake robot can be denoted by a position space G that describes the location and orientation of the robot in the world, and a shape space R that defines the relative placement of points on its body. The position of the robot is given by $g = (x, y, \theta)$ relative to a choice of origin frame, and the shape of the robot is given by $r = (\alpha_1, \alpha_2)$. We model the relationship between changes in shape and position as a *local connection* matrix $\mathbf{A}$,

$$\mathring{g} = -\mathbf{A}(r)\dot{r}$$

where $\mathring{g}$ is the system body velocity ($\dot{g}$ expressed in forward, lateral, and rotational components) and $\dot{r}$ is the rate of change of body shape. The model holds under the assumptions that gliding cannot occur and that displacement is locally proportional to the amount of shape change. A local connection matrix summarizing an appropriate dynamics model for this system can be constructed by taking a ratio between lateral and longitudinal drag forces and assuming quasistatic equilibrium [22]. The local connection matrix can be visualized as a set of vector fields on R relating changes in x, y, and θ to changes in shape $r = (\alpha_1, \alpha_2)$. Over a cyclic trajectory in the shape space (a gait), the net integral along the vector fields (i.e. the net displacement over the cycle) can be approximated by the area integral of the curvature of the constraints, $-D\mathbf{A}$, in the region enclosed by the gait. $D\mathbf{A}$ is the total Lie bracket of $\mathbf{A}$, and is closely related to its row-wise curl [23], [24].

The components of the constraint curvature $D\mathbf{A}(\alpha_1, \alpha_2)$ for the soft serpentine system are shown in Fig. 3 as contour plots, overlaid with an example gait that traverses the shape space by varying α_1 and α_2 sinusoidally and 90 degrees out of phase to produce a "circular" stroke. Note that there is an elliptical sign-definite region surrounding the origin in the contour plot for the x-component of position, whereas the y- and θ- plots have symmetric positive and negative regions around the origin. Gaits that enclose this region will thus produce net displacement along only the x-dimension of the body position. Previous work in geometric mechanics has demonstrated the utility of gait selection by choosing a stroke cycle that encloses sign-definite regions of these contour maps [17] [13] [22].

A gait cycle that encloses the entire sign-definite region should produce the largest displacement per cycle, but the shape sequence required to do this might have a high energy cost. The soap-bubble method [21] is an extension of this algorithm that attempts to optimize the gait cycle in terms of the displacement gained relative to the cost of the stroke. Curvature enclosed near the zero-contour is of low value, and so contributes relatively little to the net displacement and the shape changes required to encompass it require more time or effort in each cycle, meaning that a stroke that is contracted away from this contour is often more cost-efficient in terms of time and power.

We select gait cycles for our soft snake robot that enclose portions of the sign-definite region of the x-dimension contours of curvature to 1) demonstrate that the robot is able to achieve net longitudinal displacement with these gaits and 2) validate the displacement against the model based on the portion of sign-definite region enclosed by the cycle. The gaits tested all vary α_1 and α_2 in an elliptical stroke of the general form

$$\begin{bmatrix}\alpha_1(t)\\ \alpha_2(t)\end{bmatrix} = R(\phi)\begin{bmatrix}a\cos(t)\\ b\sin(t)\end{bmatrix} \tag{1}$$

where $2a$ and $2b$ are the widths of the major and minor ellipse axes and $R(\phi)$ is a rotation of the ellipse about the origin by an angle of ϕ.

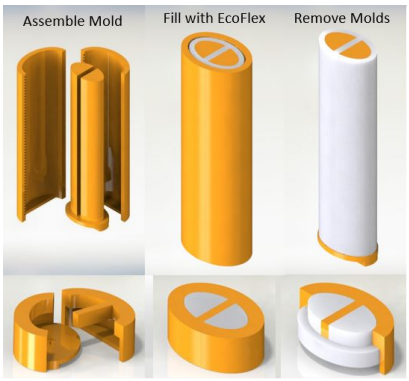

(a) Fabrication procedure

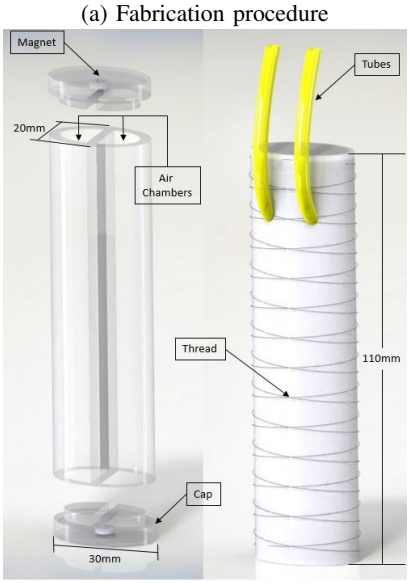

(b) Assembly and dimensions

Fig. 4: (a) Fabrication procedure to mold the silicone actuators. (b) Depiction of actuator assembly along with the final wrapping configuration and tube placement.

III. Actuator Design & Characterization

To implement the gait sequences described above, the actuators must be capable of achieving a broad set of C- and S-shaped poses (see Fig. 3(a)). Each actuator must exhibit bidirectional bending to at least a 90° arc without producing significant twisting or rolling. The snake should be modular because locomotion will require at least one pair of antagonistic actuators in tandem, thus each actuator must have a connecting mechanism that does not require excessive use of rigid parts. Fiber-reinforced actuators were selected because they have been well characterized [25], and because they are highly modifiable. A typical fiber-reinforced actuator has one chamber used for actuation. A strain-limiting layer can be added for bending, and different fiber wrapping techniques can be used for extending or twisting [26].

In order to meet the requirements above, we implemented the following designs: 1) The mold structure was modified to create two air chambers for bidirectional bending. 2) A double-helical thread wrapping pattern was used to prevent twisting upon inflation, which disrupts the gait pattern significantly enough to prevent any forward displacement. 3) An elliptical cross section geometry was selected to approximate the typical body shape of a snake, and prevent the actuators from rolling during actuation. 4) Magnets were embedded into the silicone caps used to seal the ends of the chambers, so that an arbitrary number of actuators can be linked together. Placing them in the caps prevents them from interfering with inflation. The final actuator designed is 110mm in length, and has an elliptical cross section with a semi-major axis of 30mm, semi-minor axis of 20mm, and a wall thickness of 3mm.

The soft actuators were fabricated in 3D printed molds and wrapped and assembled by hand. The mold material was MeltInk3d 2.85mm PLA printed on an Ultimaker 2+ using a 0.6mm nozzle. The actuators were made from EcoFlex®00-30. As can be seen in Fig. 4, each actuator was molded in three parts: a main body containing the air chambers and two caps with embedded magnets. The caps were glued to both ends of the main body with SilPoxy® and the seam was sealed with a thin layer of the EcoFlex®00-30. The unique design of these fiber-reinforced actuators required several iterations of fabrication improvements. Once the final fabrication method was established, we characterized each actuator to ensure they had appropriate mechanical programming to realize the shape sequence involved in a lateral undulation gait.

During the iterative prototyping and testing procedure used to determine a final design for the soft actuators, it was confirmed that actuators that perform similarly in testing reproduced the desired gait pattern better. The final fabrication process greatly reduced the number of inconsistencies between actuators, but determining how each actuator curved under a specified pressure was necessary in implementing the gait pattern correctly. We used an Optitrack Prime 13 motion capture system to track the arc angle and length of each actuator at known values of input pressure, using a syringe to inflate each chamber from 0 to 24 kPA in 3.4 kPA increments. The results of these tests are summarized by the Pressure-Angle and Pressure-Length curves for the two closest performing actuators in Fig. 5.

By quantifying the relationship between pressure and curvature, we were able to select a pair of actuators with roughly symmetrical bending behavior out of the six actuators assembled with the final design. This characterization phase was essential to ensure that the robot would be capable of bending enough to attain the pose sequences of S- and C-shaped backbones, and also provided us with a mapping between input pressure and shape that helped with tuning the control algorithms to create shape sequences.

IV. Experimental Procedure

In order to implement gait strokes and evaluate their performance, we developed methodologies for directly controlling the shape parameters α_1 and α_2 of the robotic system, tracking progression through the shape space, and measuring net displacement of the robot. The experimental procedure we followed uses a motion capture system to

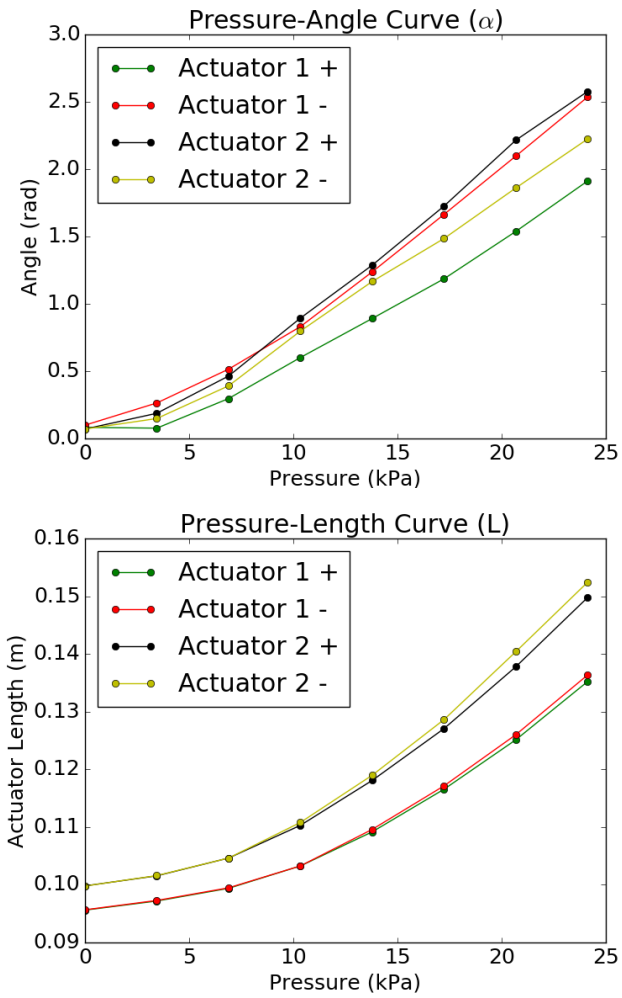

Fig. 5: Pressure-angle and pressure-elongation curves for each chamber of each actuator.

quantify the robot's shape and position changes for each gait stroke.

The snake's pneumatic control system is based on an open source design [27] that utilizes a single microcompressor with separate air lines for the actuator chambers. They can be driven to a separate pressure with solenoids valving at variable PWM rates. An Arduino Mega operates the solenoids by receiving control instructions from a separate computer via a serial data connection. Using the relationship between pressure and shape previously established, we developed Python scripts to drive PWM rates (and hence angles of curvature) sinusoidally in an appropriate pattern to realize elliptical gait stroke sequences.

We placed 4mm reflective markers in three locations on each actuator and employed the OptiTrack Prime system to monitor the bend angle and displacement of the snake. The markers were placed on the dorsal surface of each cap and at the center of the actuator's elastic spine (as seen in the shape snapshots in Fig. 6), so that the three points could be used to fit a circle to the actuator and thus yield a numerical approximation of its arc angle. The body frame of the two-actuator system was identified as the center point of the line formed by the two markers adjacent to each other where the actuators were clasped together by magnets. All motion capture data was saved and post-processed to compute and plot the body frame coordinates and curvature angles observed during a gait test.

A test area was created inside the motion capture stage by filling a large bin with millet, which was selected as the granular medium for these experiments because of its relatively low density ratio of 0.78 to 1 compared with the robot. The lateral-to-longitudinal drag ratio for the substrate was measured as 1.8 to 1. The drag ratio of the surface medium contributes considerably to net displacement, since lateral resistance translates lateral waves of bending along the backbone into forward movement, and so this ratio is crucial to estimating expected displacement.

We tested gait strokes described by Equation (1) with varying values of b and ϕ. The value of a was fixed in all tests to limit actuator bending to about 2 radians in either direction. Parameter values were selected empirically to enclose various regions within the zero-contour line, with rotations of $\phi = \frac{\pi}{4}$ or $\phi = \frac{3\pi}{4}$ to evaluate the impact of enclosing lengthwise and transverse regions of the elliptical area.

V. Results

Five different elliptical gaits were examined, with each test cycling through about 3 repetitions of a gait stroke during a total test duration of roughly 54 seconds or 18 seconds per stroke. Actual variations in shape parameters as observed with the motion capture system and calculated during post-processing of data are plotted on top of the $D\mathbf{A}^x(\alpha_1, \alpha_2)$ contour plot in Fig. 6 and Fi.g 7. The plot in Fig. 6 includes snapshots of backbone shapes that correspond to select points on the gait stroke to illustrate the pose sequence. Displacement is visualized as a function of time in Fig. 8. Net x- and y- displacement measurements for all gaits are shown in Table 9.

All gait strokes examined in these experiments achieved measurable forward displacement, and it should be noted that these gaits were within the boundaries of the sign-definite region with respect to $D\mathbf{A}^x$. For comparison with the displacement measurements observed with the motion capture system, we estimated the area integrals of $D\mathbf{A}^x$ based on the 1.8:1 drag ratio over each of the five regions enclosed by the actual shape trajectories. These predicted displacement values are also given in Table 9 in units of body lengths (L) per cycle. The cost for a gait stroke in this system was taken as the magnitude of the total shape change incurred over the cycle, which is the estimated perimeter length of the elliptical trajectory. To assess relative efficiency of each gait pattern, the average displacement was normalized against cost, and both cost and efficiency metrics are reported in Table 9 as well.

The circular stroke ($a : b = 1$) performed significantly better than the other gaits in terms of net displacement per cycle, and only somewhat better than the others in terms of efficiency. Net displacement appears to scale with size of the

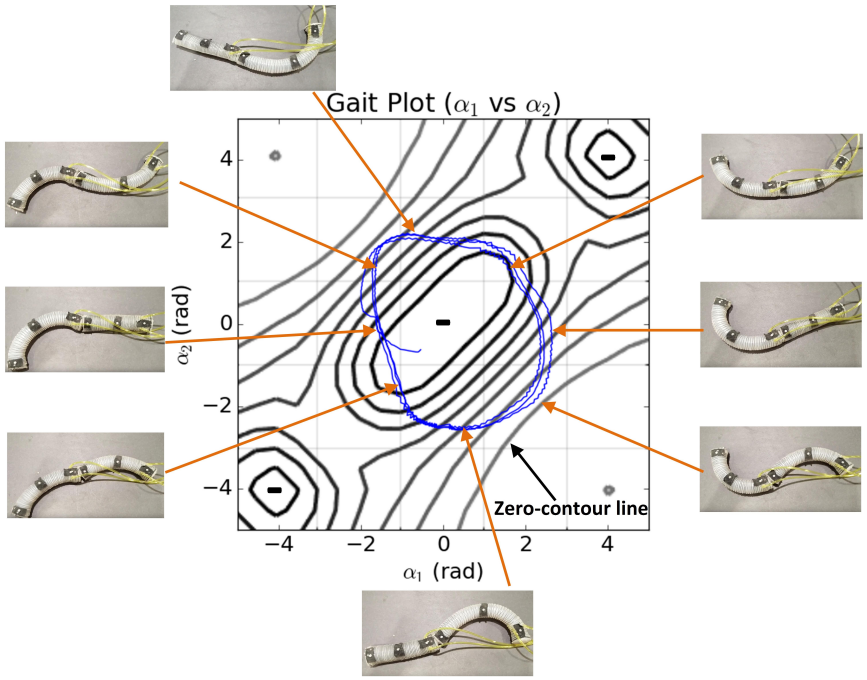

Fig. 6: Motion capture data from the soft robot demonstrating a circular gait stroke ($a : b = 1$) plotted on top of the $D\mathbf{A}_x(\alpha_1, \alpha_2)$ contour plot for the two-link soft serpenoid system. Key frames in the shape cycle are indicated with pictures.

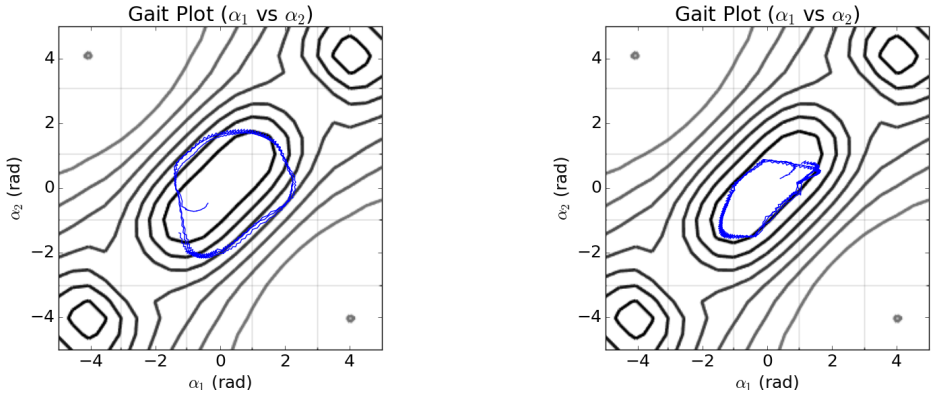

(a) $a : b = 2, \phi = \frac{\pi}{4}$ (b) $a : b = 4, \phi = \frac{\pi}{4}$

(c) $a : b = 2, \phi = \frac{3\pi}{4}$ (d) $a : b = 4, \phi = \frac{3\pi}{4}$

Fig. 7: Gait stroke plots for four different elliptical gaits collected with the motion capture system. The observed gait strokes are plotted on top of the $D\mathbf{A}_x(\alpha_1, \alpha_2)$ contour plot.

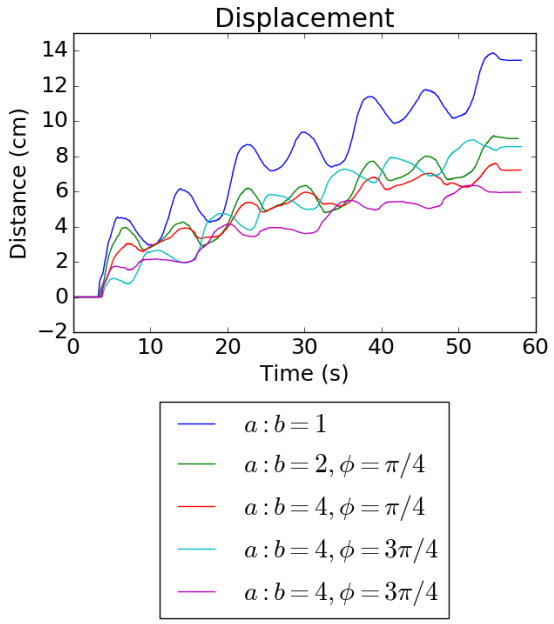

Fig. 8: Displacement along the longitudinal (x) body axis visualized as a function of time for all gait strokes examined with the motion capture system.

elliptical area enclosed about the origin and does not have a strong dependency on the orientation of that ellipse, although the elliptical gaits oriented at $\phi = \frac{\pi}{4}$ perform slightly better. It is worth noting that efficiency gains diminish as the size increases, which is consistent with the soap-bubble heuristic for gait selection. The measured displacements agree with the area integral predictions in terms of which gaits offer the most displacement, though not on the magnitude of the displacement. The soft snake actually produced more net forward movement by a factor of 2-3 over the predictions. This discrepancy is most likely attributed to a peristalsis effect caused by the cycles of elongation and retraction that accompany the bending in C- and S-shaped backbones. This explanation is also supported by the displacement plots and visual qualitative analysis of the gait, which show cycles of stretching and pulling forward on retraction. Another explanation could be that our drag coefficient measurement is incomplete which would effect the magnitude of the predicted displacement while having a minimal effect on the size of the sign-definite region.

A key trend to note across all gait plots is the contraction of the stroke curve in quadrants I and III. As shown in Fig. 6, a C-shaped backbone is produced when α_1 and α_2 have the same sign (quadrants I and III), and an S-shaped backbone when they have opposite signs (quadrants II and IV). The orientation of the elliptical sign-definite region of $D\mathbf{A}^x$ with its semi-major axis along $\alpha_1 = \alpha_2$ indicates that an "ideal" gait would include tight arc angles in the C-shapes and relatively shallow angles on the S-shapes. All gait plots gathered with motion capture show a somewhat concave curve in quadrant I, quadrant III, or both, highlighting that the soft robot was not as successful at achieving high-curvature C-shapes as it should be to perform a maximum-displacement gait stroke.

The strong S-shape backbones consistently demonstrate arc angles of about 2 radians from both actuators, which indicates that each is capable of achieving strong arcs in both positive-direction and negative direction curvature and suggests that the explanation for weaker C-shapes is unrelated to their bending capabilities. Forming a C-shape is usually a higher-cost operation than forming an S-shape of similar amplitude, since both ends of the body are moving in the same direction in a high-lateral-drag medium. We noticed the actuators pivoting slightly outwards about the magnetic fastener when forming C-shapes, probably at least partially due to this high drag force condition. Revising the clasp design to prevent this flattening of the shape could likely improve the C-shape pose by forcing the body to bend into the curve.

Additionally, the pair of actuators selected for the gait tests show some slight discrepancies in bending behavior and neither actuator is perfectly symmetrical, which could potentially be a source of error when implementing a gait pattern. A key challenge when working with soft actuators that are manufactured by molding is inconsistency in fabrication, which is difficult to avoid when using manual techniques. Fig. 5 shows enough variation in bend angle and elongation curves to potentially cause asymmetries in backbone curve.

VI. Conclusion & Future Work

We have successfully developed a modular soft snake robot that is capable of implementing gait cycles to mimic lateral undulation utilized by snakes for locomotion. By using a well-defined geometric gait model originally developed for rigid snake robots, we show that it is possible to select gaits that produce significant forward displacement separately from modeling the nonlinear dynamics of the soft actuators. The shape-space-driven design of the robot allowed for the successful realization of several parameterized gait strokes on the shape space. The performance of the gaits validated the soap-bubble method as a heuristic for selecting high-efficiency gaits, with those gaits that enclosed more of the sign-definite area yielding diminishing returns on efficiency even as the net displacement increased. The inherent properties of using soft actuators to mimic a soft-bodied animal proved advantageous for replicating serpentine locomotion, exceeding the net displacement estimates likely because of its natural tendency for peristalsis.

We plan to continue exploring shape-space-driven design with the addition of automated fabrication techniques such as 3D printing soft materials to enable production of more complex and consistent actuators. This would enable us to complete another design iteration of the actuators to improve the C-shaped backbone sequences to explore maximum-efficiency and maximum-displacement gaits. Additive manufacturing techniques could be used to investigate patterning the actuators to mimic the anisotropic friction that scales provide for biological snakes to produce interfacial traction on hard, flat surfaces. We plan to conduct similar experiments with longer chains of modular bidirectional continuum

Gait Parameters	Measured Δx	Measured Δy	Average Disp (x)	Predicted Disp (x)	Cost	Efficiency
$a:b=1$	13.5 cm	3 cm	0.23 L/cycle	0.09 L/cycle	29.91 rad	0.0077 L/rad
$a:b=2,\phi=\frac{\pi}{4}$	9.0 cm	0.6 cm	0.15 L/cycle	0.07 L/cycle	22.96 rad	0.0065 L/rad
$a:b=4,\phi=\frac{\pi}{4}$	7.3 cm	0.4 cm	0.12 L/cycle	0.03 L/cycle	17.85 rad	0.0067 L/rad
$a:b=2,\phi=\frac{3\pi}{4}$	8.7 cm	1.6 cm	0.15 L/cycle	0.06 L/cycle	23.26 rad	0.0064 L/rad
$a:b=4,\phi=\frac{3\pi}{4}$	6.0 cm	0.25 cm	0.1 L/cycle	0.03 L/cycle	20.53 rad	0.0049 L/rad

Fig. 9: Net displacements along the longitudinal (x) and lateral (y) body axes during the gait tests. The displacements are measured over 3 cycles of the gait stroke and the time elapsed for each test was roughly 54 seconds. Average displacement in body lengths (L) per cycle are also given for comparison with displacements predicted by area integral of D**A**. The gait cost is the magnitude of shape change in a cycle (estimated perimeter of the actual elliptical trajectory, measured in radians), and efficiency normalizes average displacement against the cost of the stroke.

actuators to realize more elegant backbone shapes for other serpentine gaits. There are also plans to expand the geometric mechanics model to include backbone elongation so that it can better describe peristaltic systems. Finally, we will explore the effectiveness of evolutionary/learning algorithms to provide efficient gaits by both directly searching the gait space, and by searching the parameter space of a predetermined gait profile. Overall, this work validates using a soft actuator design to realize snake-like robot locomotion and geometric mechanics model as an approach to drive design and control of a soft robot.

Contributions

CB, CF, RH, and YM designed research. CB, CF, JR, and AK performed research. CB, CF, JR, and AK analyzed data. CB, CF, JR, KT, RH, and YM wrote the paper.

Acknowledgements

This work was supported by HP Labs. We thank Will Allen, HP Fellow, and David Murphy, Distinguished Technologist, both at HP Labs, for their feedback and guidance.

References

[1] D. I. Goldman and D. L. Hu, "Wiggling Through the World - The mechanics of slithering locomotion depend on the surroundings," *American Scientist*, vol. 98, no. 4, pp. 314–323, 2010.

[2] I. S. Godage, G. A. Medrano-Cerda, D. T. Branson, E. Guglielmino, and D. G. Caldwell, "Dynamics for variable length multisection continuum arms," *The International Journal of Robotics Research*, vol. 35, no. 6, pp. 695–722, 2015.

[3] F. Largilliere, V. Verona, E. Coevoet, M. Sanz-Lopez, J. Dequidt, and C. Duriez, "Real-time control of soft-robots using asynchronous finite element modeling," *2015 IEEE International Conference on Robotics and Automation (ICRA)*, pp. 2550–2555, 2015.

[4] M. Giorelli, F. Renda, G. Ferri, and C. Laschi, "Learning the inverse kinetics of an octopus-like manipulator in three-dimensional space," *Bioinspiration & Biomimetics*, vol. 8064 LNAI, pp. 378–380, 2015.

[5] A. Iscen, A. Agogino, V. SunSpiral, and K. Tumer, "Flop and roll: Learning robust goal-directed locomotion for a tensegrity robot," in *Intelligent Robots and Systems (IROS 2014), 2014 IEEE/RSJ International Conference on*. IEEE, 2014, pp. 2236–2243.

[6] A. Iscen, K. Caluwaerts, J. Bruce, A. Agogino, V. SunSpiral, and K. Tumer, "Learning tensegrity locomotion using open-loop control signals and coevolutionary algorithms," *Artificial life*, 2015.

[7] R. F. Shepherd, F. Ilievski, W. Choi, S. a. Morin, A. A. Stokes, A. D. Mazzeo, X. Chen, M. Wang, and G. M. Whitesides, "Multigait soft robot," *Proceedings of the National Academy of Sciences*, vol. 108, no. 51, pp. 20 400–20 403, 2011.

[8] M. T. Tolley, R. F. Shepherd, B. Mosadegh, K. C. Galloway, M. Wehner, M. Karpelson, R. J. Wood, and G. M. Whitesides, "A Resilient, Untethered Soft Robot," *Soft Robotics*, vol. 1, no. 3, pp. 213–223, 2014.

[9] A. A. Calder, J. C. Ugalde, J. Crist, and O. P, "Design , Fabrication and Control of a Multi-Material – Multi-Actuator Soft Robot Inspired by Burrowing Worms."

[10] T. Umedachi, V. Vikas, and B. A. Trimmer, "Highly deformable 3-D printed soft robot generating inching and crawling locomotions with variable friction legs," *IEEE International Conference on Intelligent Robots and Systems*, pp. 4590–4595, 2013.

[11] S. Hirose, *Biologically inspired robots: snake-like locomotors and manipulators*. Oxford University Press, 1993.

[12] M. Tesch, K. Lipkin, I. Brown, R. Hatton, A. Peck, J. Rembisz, and H. Choset, "Parameterized and Scripted Gaits for Modular Snake Robots," *Advanced Robotics*, vol. 23, pp. 1131–1158, 2009.

[13] R. L. Hatton, Y. Ding, H. Choset, and D. I. Goldman, "Geometric visualization of self-propulsion in a complex medium," *Physical Review Letters*, vol. 110, no. 7, 2013.

[14] G. S. Chirikjian and J. W. Burdick, "Kinematically Optimal Hyper-Redundant Manipulator Configurations," *IEEE Transactions on Robotics and Automation*, vol. 11, no. 6, pp. 794–806, 1995.

[15] C. Wright, A. Johnson, and A. Peck, "Design of a modular snake robot," *IEEE/RSJ International Conference on Intelligent Robots and Systems, 2007.*, pp. 2609–2614, 2007.

[16] C. Wright, A. Buchan, B. Brown, J. Geist, M. Schwerin, D. Rollinson, M. Tesch, and H. Choset, "Design and architecture of the unified modular snake robot," *Proceedings - IEEE International Conference on Robotics and Automation*, pp. 4347–4354, 2012.

[17] J. Dai, H. Faraji, C. Gong, R. L. Hatton, D. I. Goldman, and H. Choset, "Geometric Swimming on a Granular Surface," *Proceedings of Robotics: Science and Systems*, 2016.

[18] T. Ohm, "JPL Serpentine Robot: a 12 DOF System for Inspection," *Jet Propulsion*, pp. 1–5.

[19] R. L. Hatton and H. Choset, "Generating gaits for snake robots: Annealed chain fitting and keyframe wave extraction," *Autonomous Robots*, vol. 28, no. 3, pp. 271–281, 2010.

[20] C. D. Onal and D. Rus, "Autonomous undulatory serpentine locomotion utilizing body dynamics of a fluidic soft robot," *Bioninspiration & Biomimetics*, 2013.

[21] S. Ramasamy and R. L. Hatton, "Soap-bubble Optimization of Gaits," 2016.

[22] R. Hatton and H. Choset, "Geometric Swimming at Low and High Reynolds Numbers," *IEEE Transactions on Robotics*, no. June, pp. 1–10, 2013.

[23] R. L. Hatton and H. Choset, "Geometric motion planning: The local connection, Stokes' theorem, and the importance of coordinate choice," *The International Journal of Robotics Research*, vol. 30, pp. 988–1014, 2011.

[24] ——, "Nonconservativity and noncommutativity in locomotion: Geometric mechanics in minimum-perturbation coordinates," *European Physical Journal: Special Topics*, vol. 224, no. 17-18, pp. 3141–3174, 2015.

[25] P. Polygerinos, Z. Wang, J. T. B. Overvelde, K. C. Galloway, R. J. Wood, K. Bertoldi, and C. J. Walsh, "Modeling of Soft Fiber-Reinforced Bending Actuators," *IEEE Transactions on Robotics*, 2015.

[26] F. Connolly, P. Polygerinos, C. J. Walsh, and K. Bertoldi, "Mechanical Programming of Soft Actuators by Varying Fiber Angle."

[27] "Soft Robotics Toolkit."